

This is an Open Access document downloaded from ORCA, Cardiff University's institutional repository:<https://orca.cardiff.ac.uk/id/eprint/147967/>

This is the author's version of a work that was submitted to / accepted for publication.

Citation for final published version:

Kim, Yeongha, Wong, Stephan, Seo, Changwon, Yoon, Jeong Hoon, Choi, Gwan Hyun, Olthaus, Jan, Reiter, Doris E., Kim, Jeongyong, Kim, Teun-Teun, Oh, Sang Soon and Gi-Ra, Yi 2022. Self-assembled honeycomb lattices of dielectric colloidal nanospheres featuring photonic Dirac cones. *ACS Applied Nano Material* 5 (3) , pp. 3386-3393. 10.1021/acsanm.1c03986

Publishers page: <https://doi.org/10.1021/acsanm.1c03986>

Please note:

Changes made as a result of publishing processes such as copy-editing, formatting and page numbers may not be reflected in this version. For the definitive version of this publication, please refer to the published source. You are advised to consult the publisher's version if you wish to cite this paper.

This version is being made available in accordance with publisher policies. See <http://orca.cf.ac.uk/policies.html> for usage policies. Copyright and moral rights for publications made available in ORCA are retained by the copyright holders.



# Self-assembled Honeycomb Lattices of Dielectric Colloidal Nanospheres Featuring Photonic Dirac Cones

*Yeongha Kim<sup>a,‡</sup>, Stephan Wong<sup>b,‡</sup>, Changwon Seo<sup>c,‡</sup>, Jeong Hoon Yoon<sup>a</sup>, Gwan Hyun Choi<sup>a</sup>, Jan Olthaus<sup>d</sup>, Doris E. Reiter<sup>d</sup>, Jeongyong Kim<sup>e</sup>, Pil J. Yoo<sup>a</sup>, Teun-Teun Kim<sup>c\*</sup>, Sang Soon Oh<sup>b\*</sup>, Gi-Ra Yi<sup>a,f\*</sup>*

<sup>a</sup> School of Chemical Engineering, Sungkyunkwan University (SKKU), Suwon 16419, Republic of Korea.

<sup>b</sup> School of Physics and Astronomy, Cardiff University, Cardiff CF24 3AA, United Kingdom.

<sup>c</sup> Department of Physics and Energy Harvest-Storage Research Center (EHSRC), University of Ulsan, Ulsan 44610, Republic of Korea.

<sup>d</sup> Institute of Solid State Theory, University of Münster, 48149 Münster, Germany

<sup>e</sup> Department of Energy Science, Sungkyunkwan University, Suwon 16419, Republic of Korea

‡Department of Chemical Engineering, Pohang University of Science and Technology  
(POSTECH), Pohang, Gyeongbuk 37673, Republic of Korea

\*Corresponding authors

E-mail: [yigira@postech.ac.kr](mailto:yigira@postech.ac.kr) (G.-R.Y.), [ohs2@cardiff.ac.uk](mailto:ohs2@cardiff.ac.uk) (S.S.O.), [tkim@ulsan.ac.kr](mailto:tkim@ulsan.ac.kr) (T.-  
T.K.)

‡ Y.K, S.W, and C.S contributed equally to this paper

## **ABSTRACT**

The prime example of a two-dimensional photonic crystal featuring Dirac cones is based on the honeycomb lattice. Colloidal self-assembly can produce a two-dimensional colloidal structure over a large area, but is limited to hexagonal-close-packed structures. Therefore, it has been challenging to fabricate honeycomb monolayers by colloidal self-assembly. Here, we fabricate a dielectric honeycomb lattice in a large area by template-assisted self-assembly and analyze its photonic structure. Although the Dirac point occurring at the K point is not accessible by light in free space, a part of the upper Dirac cone above the light line is verified by a Fourier analysis of the back-focal plane image. Since the template-assisted self-assembly enables additional geometrical perturbations in the honeycomb lattice, various lattices can be fabricated. This additional degree of freedom may provide an alternative way of fabricating photonic topological insulators.

**KEYWORDS:** Photonic crystal, Honeycomb, Fourier plane, Dirac cone

## INTRODUCTION

A honeycomb lattice is the hexagonal lattice with a two-atomic basis, in which the centers of the hexagons form a hexagonal lattice. Because by geometric perturbations a topological edge mode is easily obtained,<sup>1</sup> the honeycomb lattice has recently attracted substantial attention displaying unique properties such as low-loss unidirectional light propagation<sup>2,3</sup> and topologically protected lasing.<sup>4,5</sup> So far, in experimental reports, honeycomb lattice has been fabricated primarily in top-down methods<sup>6-9</sup> which are, however, time-consuming and costly. Alternatively, bottom-up approaches produce uniform nanostructures of colloidal particles in large-area at low cost,<sup>10-12</sup> but specially-designed colloidal particles such as tri-patch particles<sup>13</sup> or DNA-coated particles<sup>14,15</sup> are needed as building blocks for those honeycomb lattice. As reported, the synthesis of submicrometer-sized tri-patch particles require elaborate experimental control<sup>15</sup> and is time consuming, while DNA-mediated assembly requires accurate control of the experimental conditions including salt concentration and temperature.<sup>16</sup> Since those special colloidal particles are assembled in a liquid, an additional transfer step to a substrate is necessary for optical measurements. In case of spherical particles, using self-assembled colloidal monolayers, a honeycomb lattice was formed but only in a limited area.<sup>16</sup> Of course, such structures would not be obtained by co-self-assembly of binary mixtures,<sup>17,18</sup> either.

For further development of self-assembled structures into photonic devices, it is important to analyze the optical modes in those structures. Commonly, angle-resolved reflection and transmission spectroscopy is used to characterize the optical modes above the light-line.<sup>19,20</sup> However, measurement of angular distributions of light reflection/transmission is highly

challenging due to the requirement of rather large samples and the low coupling efficiency into the optical modes. Alternatively, Fourier-plane spectroscopy has been used to directly measure photonic band structures of a hexagonal lattice of metallic nano particle arrays<sup>21</sup> and a one-dimensional metallic grating.<sup>22</sup> In this method, a wide range of angular components of the reflected light beam are collected by a high numerical aperture (NA) objective lens and then mapped onto an image at the back focal plane showing the momentum space distribution of the light.

In this report, we demonstrate a large-area dielectric honeycomb lattice of dielectric nanospheres on nanoimprinted patterned polymeric templates. By convective assembly, nanospheres form densely packed multilayers and then nanospheres in bottom layer are strongly adhered on the patterned polymer layer by subsequent thermal annealing. The optical properties of the honeycomb lattice characterized by directly measuring the reflectance spectra and mapping image in the Fourier-plane. Furthermore, the Dirac cone, which originates from the  $C_3$  symmetry of the honeycomb lattice, is investigated by analyzing the Fourier-plane mapping image of the fabricated samples. Because the access to the Dirac point is limited by the free space excitation in the reflectance measurement setup, we are able to measure a part of the Dirac cone above the light line.

## **METHODS**

**Synthesis Silica Nanospheres.** Silica nanospheres are prepared by the Stöber method.<sup>23</sup> This is an ammonia-catalyzed sol-gel reaction, so it helps making the monodisperse silica nanospheres. Tetraethyl orthosilicate (TEOS, Sigma Aldrich,  $\geq 99\%$ ) is hydrolyzed in the presence of distilled water and ethanol. By changing the amount of solvent (ethanol, SAMCHUN, 99.9%), we can easily control the size of silica nanospheres. To synthesize the silica nanospheres which have 160, 250, and 400 nm diameters, we first mix 200, 150, and 90 ml of ethanol, fixed amounts of 7.5 ml water, and 20 ml ammonia with vigorous stirring. After 1 hour, we add 15 ml of TEOS to the solution. The reaction is terminated about 3 hours later. To prevent unreacted monomers from further reacting and to make the non-uniform particles, we perform a process of washing with ethanol for more than 4 times.

**Patterned Substrate Fabrication.** The polymeric nano-scale hexagonal array is fabricated using capillary force lithography. A glass substrate is prepared ( $2 \times 2 \text{ cm}^2$ ) and washed by distilled water followed isopropyl alcohol (SAMCHUN, 99.5%) for more than 5 minutes. After blowing the substrates with  $\text{N}_2$  gas, a thermal evaporator system (Dae-Dong High Tech.) is used to deposit metal layers. After chromium<sup>24</sup> layer with a thickness of 10 nm, which has the role of an adhesion layer between the glass and the next layer, a gold layer with a thickness of 50 nm is deposited. Then, the gold coated substrate is washed by sonicating in isopropyl alcohol and distilled water. Next, 3 wt % of Polystyrene (Sigma Aldrich,  $M_w = 170,000$ ) in toluene (Sigma Aldrich, 99.8%) is spin coated on the gold substrates at 3000 rpm for 20 seconds. The annealing process is needed to obtain a smooth surface, and completely evaporate the toluene solution. The procedure for the capillary force lithography (CFL) uses the capillary force material (CFM).<sup>25</sup> CFM molds are fabricated twice by replicating silicon master mold which is made by e-beam lithography, having a hexagonal array, by UV-exposure process with

polyurethane acrylate (PUA) resin (PSM-3080, CFM-110S). After that, we press CFM mold with a glass substrate and a transparent PDMS substrate (SILGARD184, curing-agent: elastomer = 1:10), which is the buffer layer on the prepared substrate. Above glass transition temperature ( $T_g = 95$  °C) of polystyrene, the spin coated polystyrene layer will be melted and capillary risen in CFM molds. After cooling the substrates, CFM molds are removed by sharp tweezers.

**Honeycomb Lattice Fabrication.** In the convective assembly, highly dense nanospheres can be accumulated on the patterned substrates.<sup>16</sup> 1 wt % of the silica nanospheres in ethanol are slowly evaporated<sup>26</sup> at room temperature. When silica nanospheres are mono-dispersed, they will assemble in close-packing. After complete evaporation, the substrate is annealed above the  $T_g$  of the polystyrene. After this process, the polystyrene patterns are slightly melted, and hold the bottom of silica nanospheres.<sup>27</sup> The substrate is cooled to room temperatures and sonicated for 40 seconds. The upper layers are detached from the substrate except the bottom layer, which is held by the polystyrene pattern. Therefore, we can see the honeycomb lattice with silica nanospheres.

**Numerical Simulations.** To draw the photonic band structure of the freestanding dielectric nanosphere array (Figure 1a) and the nanosphere on top of the substrate including the gold layer (Figure 1b), we use MPB<sup>28</sup> and an FDTD solver,<sup>29</sup> respectively. In the 3D MPB simulation, we calculated the TE/TM-like modes using a  $1 \times 1 \times 8$ -unit cell with Bloch periodic boundary conditions. For the nanosphere array on top of substrate with the gold layer, the TE/TM-like modes are coupled leading to hybrid modes and metallic material dispersion, which needs to be considered. Therefore, we use an FDTD method, where we apply Bloch periodic boundary conditions and excite all possible modes using an electric dipole excitation.

The refractive index used for the polymer is  $n_{PS} = 1.59$ , while the dispersive refractive index of glass and gold area used from the Palik<sup>30</sup> and the Johnson and Christy database,<sup>31</sup> respectively. The chromium layer is neglected in the simulations without loss of generality. The angle-resolved spectra (Figure 4d,e) have been obtained using the FDTD method, where a plane wave source and a frequency-domain power monitor are positioned on top of the design.

**Optical Measurement.** The angle-resolved reflectivity of the honeycomb lattice has been obtained by a lab-made back focal plane (BFP) spectroscopy set-up based on a lab-made confocal microscope system. The collimated white light source (halogen lamp, Nikon, Inc., LV-LH50PC) matches the beam spot size with a pupil of an objective lens by using a mechanical iris that is focused onto the honeycomb lattice by a 100 × objective lens with 0.9 NA. The reflected light is collected by the same objective lens. The angle-resolved reflected light focused on the BFP of the objective lens is imaged on a complementary metal oxide semiconductor camera (CMOS camera, Thorlabs, DCC 1645C) at the Fourier plane by using an extra tube lens with a 200 mm focal length placed between a tube lens in the confocal microscope system and the CMOS camera. The angle-resolved reflectance spectra are measured by collecting the focused angle-resolved light onto the Fourier plane using an optical fiber with a 100 μm core diameter, which works as a confocal detection pinhole, and then guided to a spectrometer (Princeton instruments, Inc., Acton SpectraPro-500) equipped with the charged-coupled device camera (CCD, Princeton instruments, Inc., PIXIS 100B). The BFP scan image is measured by a lab-made pinhole scan system, which combined the pinhole and three-axis step motorized stage. The spectrometer is electrically synchronized with the pinhole installed motorized stage; thus, a reflectance spectrum is obtained at every pixel position, and a map of the reflectance is obtained by scanning the Fourier plane with a 2 mm by 2 mm square area at 64 by 64 pixels. The reflectance maps are imaged by a filtering process (lower and upper

average background) in WITec software, which calculates the baseline points in selected frequency ranges.<sup>32</sup>

## RESULTS AND DISCUSSION

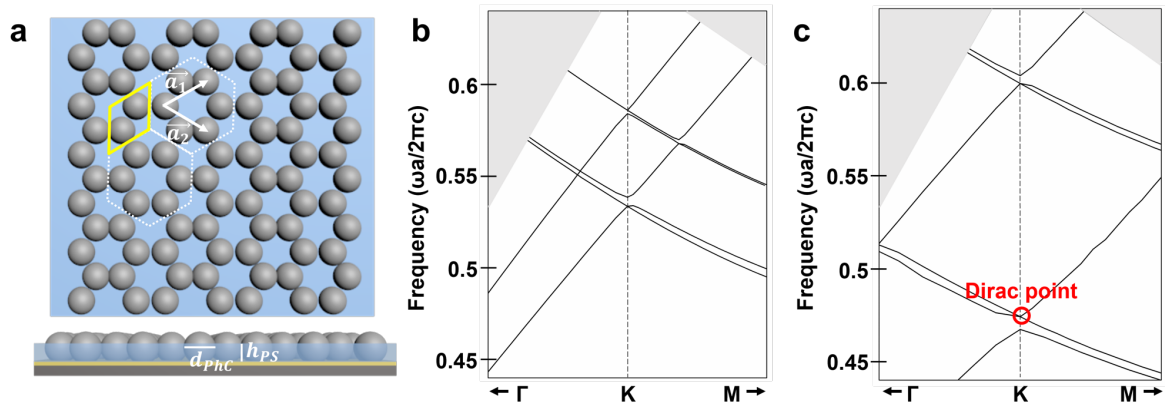


**Figure 1.** (a) Schematic of the proposed honeycomb lattice with top and cross section views. ( $d_{PhC} = 400$  nm,  $h_{PS} = 300$  nm). The primitive unit cell is represented by the solid yellow line and the lattice vectors  $a_1$  and  $a_2$ . Simulations of the photonic band structure (b) without (free standing) and (c) with substrate and gold layer. The grey shaded area represents the light cone in air.

Figure 1a illustrates the proposed honeycomb lattice, which is expected to have Dirac points at the K and K' points due to the  $C_3$  symmetry present in the honeycomb lattice. Besides, because the nanospheres are embedded in a polystyrene (PS) matrix, two Dirac points at similar frequencies are present at the K and K' points instead of one. With a lattice constant (a) of 700

nm, honeycomb lattice of silica nanospheres ( $d_{phc} = 400$  nm,  $n = 1.45$ ) are embedded in a polystyrene layer ( $h_{ps} = 310$  nm) on top of thin gold layer ( $\sim 50$  nm), and a glass substrate (Figure 1a). In addition, a 10 nm chromium layer is put below the gold layer as an adhesion layer.<sup>24</sup> Notably, a residual polystyrene thin layer ( $\sim 10$  nm) forms on the gold layer during the imprinting process, which results in a dielectric gap layer between the silica nanospheres and the gold-coated substrate.

Figure 1b shows the calculated band structure of the freestanding honeycomb lattice, namely without gold layer and substrate. The band structure has two Dirac points at the K point. However, these modes are above the light line of substrate, in which light may leak into the substrate. Therefore, a gold layer is introduced to confine these photonic crystal modes at the surface of the structure. The calculated band structure including the gold layer and the substrate is presented in Figure 1c. Again, the band structure features the two Dirac points at the K point, but now below the light cone.

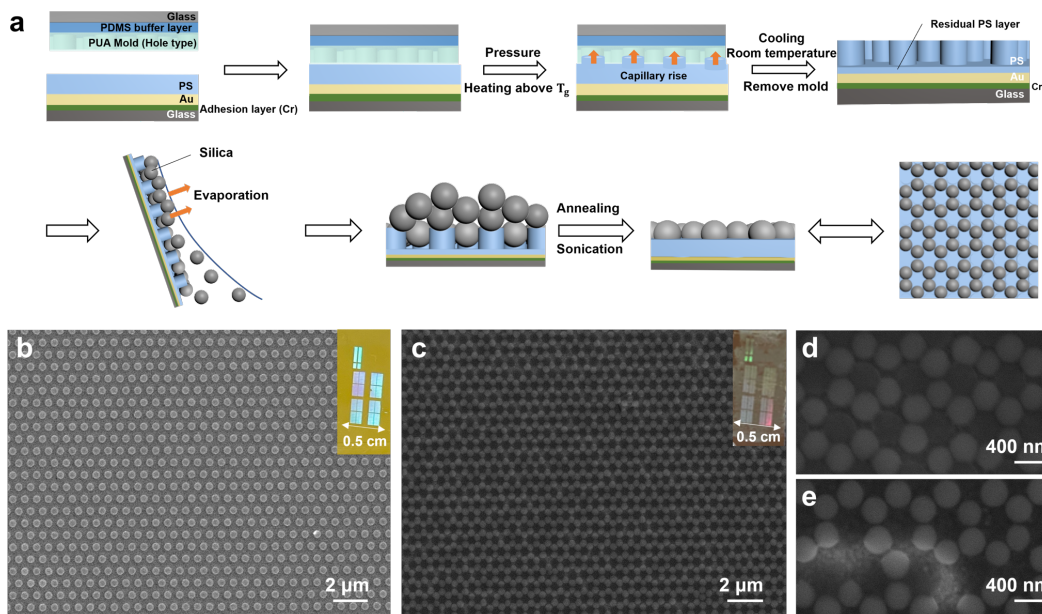


**Figure 2.** (a) Schematic illustration of the preparation of the sample. SEM image of (b) the polystyrene hexagonal-array pattern (without silica nanospheres yet) and (c) silica honeycomb lattice. (d) SEM image of silica honeycomb lattice in higher magnification, and (e) some parts have deformation. Insets in (b, c) show real sample images.

Using the techniques described in method section, we fabricate the sample with the steps shown in Figure 2. After the synthesis of the monodisperse silica nanospheres (Figure S4),<sup>23,33</sup> Figure 2a shows that steps of the patterned substrate<sup>25,34</sup> fabrication resulting in the honeycomb lattice.<sup>26,35</sup> We confirmed that the chromium and gold layers were well deposited in 10, 50 nm through energy-dispersive X-ray spectroscopy (EDS) mapping images (Figure S1). In addition, the cross-sectional SEM image of honeycomb lattice demonstrated that silica nanospheres were located between the annealed hexagonal pattern.<sup>27</sup>

To find the optimized size of silica nanospheres for honeycomb lattice, we conducted the fabrication on the polystyrene hexagonal-array pattern substrate with different sizes of silica nanospheres ( $d_{phC} = 160, 250, \text{ and } 400 \text{ nm}$ ), as shown in Figure S2. The nanospheres are filled into the space between the polystyrene hexagonal-array patterns. The silica nanospheres with size 160 nm and 250 nm are randomly arranged without any arrayed structures and arranged into other arrayed structure, respectively. The silica nanospheres with 400 nm diameter formed a honeycomb lattice.

As demonstrated in scanning electron microscope (SEM) images (Figure 2b,c), uniform silica honeycomb lattice trapped on partially melted polystyrene pattern are fabricated in more than

$20\ \mu\text{m} \times 20\ \mu\text{m}$ , which is much larger than patterns by top-down approach in previous reports.<sup>36,37</sup>

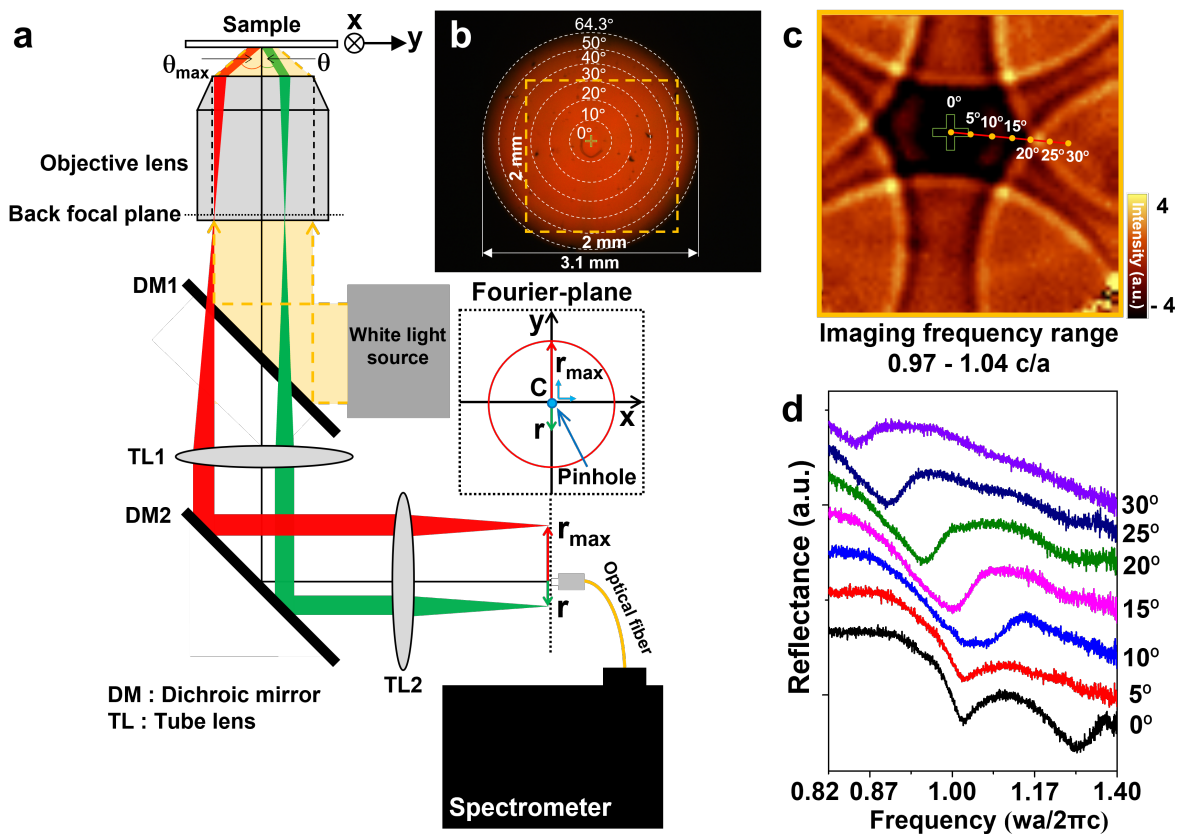


**Figure 3.** (a) Schematic picture of the Fourier-plane spectroscopy setup. By scanning the detection pinhole placed in the Fourier-plane (blue circle), the reflectance spectrum at a specific angle can be obtained. (b) Optical image of the Fourier-plane of the honeycomb lattice of silica nanospheres ( $d_{phc} = 400\ \text{nm}$ ,  $n = 1.45$ ). The reflection angles are indicated by the dashed circles in the Fourier-plane image. (c) Reflectance mapping images obtained by scanning the yellow dashed area in the Fourier-plane image. The reflectance maps are imaged

by accumulating frequency range of 0.97 – 1.04 c/a. (d) Angle-resolved white light reflectance spectra at the yellow points arrayed on red solid line in (c).

The set-up of the angle-resolved optical reflectance of the silica honeycomb lattice measured by our lab-made Fourier-plane spectroscopy is shown in Figure 3a. The angle-resolved reflected light with the beam path is indicated by red ( $\theta_{\max}$ ) and green ( $\theta$ ) color in Figure 3a from the honeycomb surface is focused at the back focal plane in the objective lens and then collimated by the tube lens (TL1) and refocused in the Fourier-plane by TL2. Subsequently, by placing an optical fiber working as a detection pinhole in the Fourier-plane, the angle-resolved reflected light focused on a specific position in the Fourier-plane is collected, and then guided to a spectrometer (see Methods for details). The reflectance spectrum is obtained by normalizing the angle-resolved reflected spectrum to the background reflected spectrum of the non-patterned gold film. Both spectra are taken at the same position in the Fourier-plane.

We measure the reflectance mapping image and representative spectra depending on the reflection angle in the honeycomb lattice. The relationship between a reflected angle ( $\theta$ ) of light at the sample and a distance ( $r$ ) from the center (green cross) to a specific position on circles displayed in the Fourier-plane (Figure 4b) is calculated by the following equation<sup>38</sup> :

$$\theta = \sin^{-1} \left( \frac{r}{r_{\max}} \times \frac{\text{NA}}{n} \right)$$

Here,  $n$  represent the refractive index of air, and  $r_{\max}$  is the maximum distance from the center, which can be observed at the Fourier plane. We used a 100 × objective lens with 0.9 NA for

focusing the incident light to the sample. Figure 3b displays an optical image of the Fourier plane. The angle of the reflected light is marked as dashed white circles in the Fourier plane image with distance  $r$ . The maximum collectable angle of reflected light is  $64.3^\circ$  for 0.9 NA, thus, we assume that the maximum size  $r_{max}$  of the Fourier plane corresponds to  $\theta_{max} = 64.3^\circ$ . Figure 3c represents the reflectance mapping image of the honeycomb lattice of silica nanospheres ( $d_{phc} = 400$  nm,  $n = 1.45$ ) by scanning the pinhole at the yellow dashed area in Figure 3b. The map is imaged by accumulating reflectance spectra with a frequency range of 0.97-1.04  $c/a$ . Figure 3d show the reflectance spectra which are obtained from the yellow points on the red solid line in Figure 3c. The dip positions of reflective angle at  $0^\circ$  are observed at 1.02  $c/a$  and 1.28  $c/a$ , respectively. The dip position at 1.02  $c/a$  remains unchanged up to a reflective angle of  $10^\circ$ , it then shifts gradually reaching 0.85  $c/a$  at  $30^\circ$ . On the other hand, the dip position at 1.28  $c/a$  disappears with increasing reflective angle.

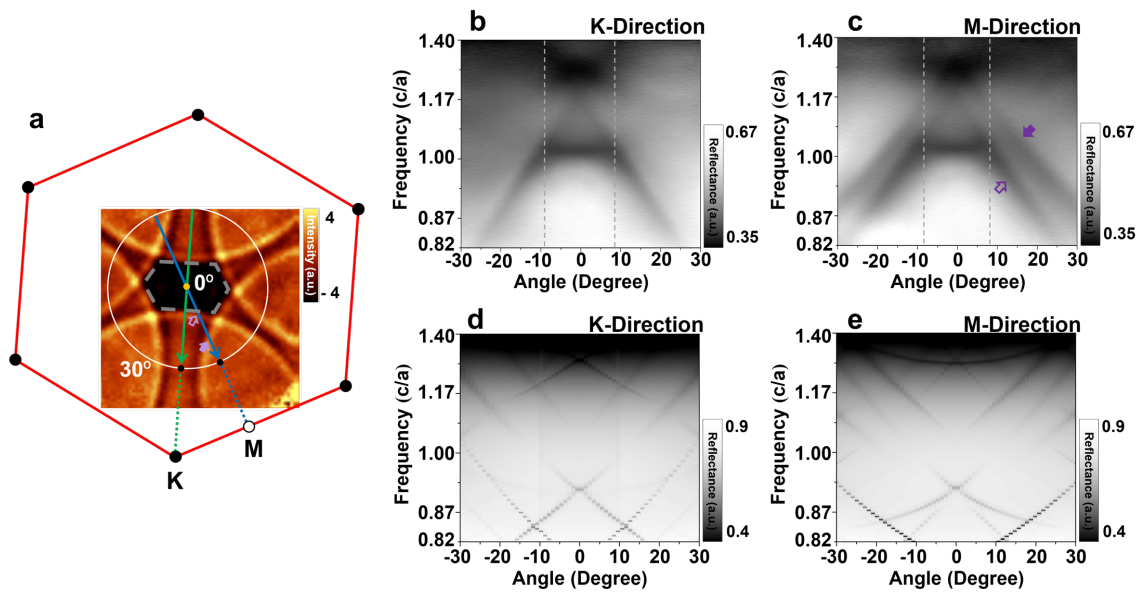


**Figure 4.** (a) The 1st Brillouin zone (red hexagon) and reciprocal lattice point (black dots) of the honeycomb lattice. Green and blue solid arrow are for identifying the K and M points, respectively (green and blue dotted lines are an extension line reach to K and M point, respectively). The inset image is obtained by accumulating a frequency range from 1.00  $c/a$  to 1.07  $c/a$ , and the gray dashed hexagon presents the iso-frequency (1.02  $c/a$ ) contour. (b)-(c) measured, and (d)-(e) simulated dip frequency dispersion image along the K (green solid arrow) and M (blue solid arrow) direction with the range of reflection angle from  $-30^\circ$  to  $30^\circ$  (white solid circle) including  $0^\circ$  (orange point), respectively.

Because the position of the diffraction circle in the Fourier plane is given by the honeycomb lattice, the 1st Brillouin zone should also display a honeycomb lattice (Figure S5). Figure 4a shows the 1st Brillouin zone (red hexagon) and iso-frequency contour (gray dashed hexagon) of the honeycomb. Both hexagons are stretched sideways due to lattice deformation which breaks the  $C_3$  symmetry and the  $C_2$  symmetry remains as demonstrated in Figure 2e. Figure 4b, c show the dip frequency dispersion image obtained by the reflectance spectra along the K (green arrow) and M (blue arrow) direction with the reflection angle range from  $-30^\circ$  to  $30^\circ$  including  $0^\circ$ , respectively. Here, the gray dashed line represents the boundary of the iso-frequency hexagon (gray dashed line in Figure 4a). The dip frequency at 1.02  $c/a$  is maintained, while the higher dip frequency is gradually reduced when increasing the distance from center ( $0^\circ$ ) to the iso-frequency boundary (gray dashed line). The outer side of the iso-frequency hexagon, the dip frequency at 1.02  $c/a$  is gradually reduced in all direction. Interestingly, compared to the dip frequency dispersion along the K direction, two lines are observed in M direction (solid and filled purple arrows in Figure 4a, c). It is also marked in Figure 4a (solid

and filled purple arrows) that the K direction only passes through one of diffraction circle, while the M direction is not. The simulation results of the dip frequency dispersion along the K and M direction, are presented in Figure 4d,e. The simulation is in good agreement with the experimental findings, as several key features of the measurements, especially the cone-like behavior of the dips, is reproduced.

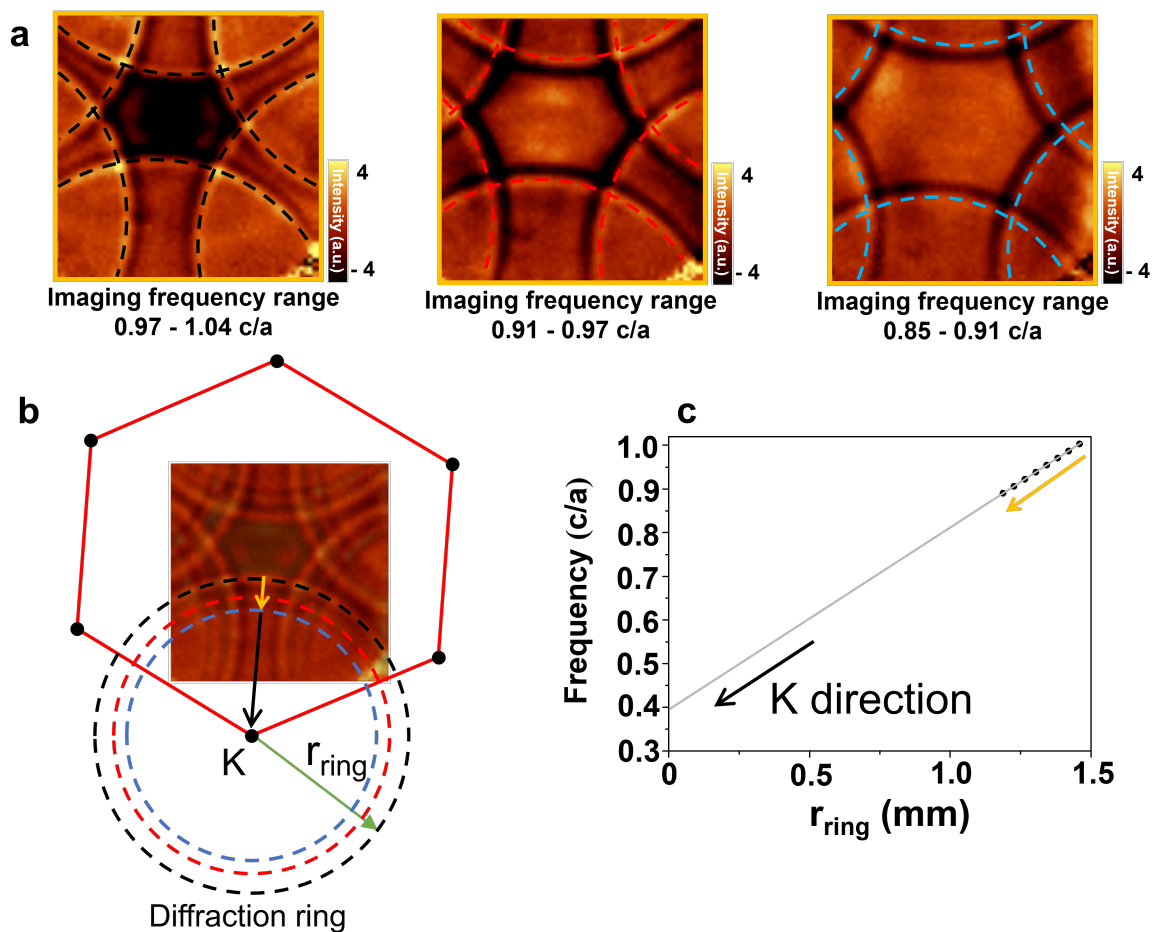


**Figure 5.** (a) Reflectance maps of the honeycomb lattice imaged by accumulating different frequency ranges with  $0.97 - 1.04 c/a$  (left),  $0.91 - 0.97 c/a$  (middle), and  $0.85 - 0.91 c/a$  (right), respectively. Black, red, and blue dashed arcs represent a part of the diffraction ring

centered at the K point (Figure S5). (b) Overlap image of (a) with diffraction rings. The radius ( $r_{ring}$ , green arrow) of the diffraction ring is observed in a frequency at 1.00  $c/a$  (black dashed ring), 0.95  $c/a$  (red dashed ring), and 0.89  $c/a$  (blue dashed ring). (c) The plot of frequency vs. radius ( $r_{ring}$ ) with the data points obtained by following yellow arrow in (b) (from black dashed ring to blue dashed ring). Black arrow and gray line represent the direction of the K point on a reciprocal lattice and the extrapolated line of the data points, respectively.

The reflectance maps of the honeycomb lattice imaged by different frequency ranges with 0.97 – 1.04  $c/a$  (left), 0.91 – 0.97  $c/a$  (middle), and 0.91 – 0.85  $c/a$  (right) is presented in Figure 5a, while, Figure 5b marks concentric rings at the Fourier plane for different frequencies. All the rings are centered at the K point on a reciprocal lattice (Figure S5), they appear as arcs in the Fourier plane image in our reflection measurement setup (Figure 5a), because the NA is too small to cover the reflected beam with the first diffraction order. Note that the origin of the rings are different from the rings that were previously reported on honeycomb lattice<sup>39,40</sup> because we do not observe a ring with the same radius around the  $\Gamma$  point. Remarkably, the radius of the circle centered at the K point is reduced when the frequency gets smaller, suggesting that this is a part of Dirac cone. It is important to note that our free space reflection measurement set-up forbids the excitation of the Dirac point that is below the light line. However, the upper Dirac cone (Figure 1c) extended to the region above the light line allows for a free space excitation and a measurement of reflected beam.

To confirm that the rings are indeed a part of the upper Dirac cone, we plot frequency vs radius together with the data from the reflectance mapping image. The Dirac point is a point degeneracy with a linear dispersion in the two-dimensional momentum space and divides the adjacent bands into two Dirac cones. Below, we call them upper and lower Dirac cones for higher and lower frequencies, respectively. In Figure 5c, the data points clearly demonstrate a linear relationship, meaning that the dispersion is linear, and the extrapolated line crosses the frequency axis at around  $0.39 c/a$ , which exhibits a good agreement with the value obtained in the numerical simulation (Figure 1c). It is worth to note that only the small part of the upper Dirac cone above the light line can be observed with incident/reflection beams from/to the free space because the Dirac point is below the light line and the area of observable upper Dirac cone is limited by the NA of the objective lens, in our case.

## CONCLUSIONS

We have fabricated a silica nanosphere honeycomb lattice using convective assembly assisted by nanoimprinted pattern. The formation of a pattern-assisted structure opens the possibility of designing more diverse structures. We have measured the photonic band structure through reflection spectra of the honeycomb structured samples, showing a qualitative agreement with numerical simulations and an anisotropic dispersion coming from the lattice deformation. Most importantly, we have observed part of the upper Dirac cone above the light line using the reflection measurement with a Fourier image. Thus, we believe that the pattern-assisted convective self-assembly method can provide diverse structures for the realization of two-dimensional photonic topological insulators.

## **ACKNOWLEDGMENTS**

This research was supported by the National Research Foundation of Korea (NRF) (No. NRF-2019R1A6A11053838, 2021R1C1C1006316, 2021R1A2C3013800). The work is partially funded by the European Regional Development Fund through the Welsh Government (80762-CU145 (East)).

## **AUTHORS' INFORMATION**

\*Corresponding authors

E-mail: yigira@postech.ac.kr (G.-R.Y.), ohs2@cardiff.ac.uk (S.S.O.), ttkim@ulsan.ac.kr (T.-T.K.)

‡ These authors contributed equally.

## REFERENCES

- (1) Wu, L. H.; Hu, X. Scheme for Achieving a Topological Photonic Crystal by Using Dielectric Material. *Phys. Rev. Lett.* **2015**, *114* (22), 223901.
- (2) Poo, Y.; Wu, R. X.; Lin, Z.; Yang, Y.; Chan, C. T. Experimental Realization of Self-Guiding Unidirectional Electromagnetic Edge States. *Phys. Rev. Lett.* **2011**, *106* (9), 093903.
- (3) Yang, J. K.; Hwang, Y.; Oh, S. S. Evolution of Topological Edge Modes from Honeycomb Photonic Crystals to Triangular-Lattice Photonic Crystals. *Phys. Rev. Res.* **2021**, *3* (2).
- (4) Harari, G.; Bandres, M. A.; Lumer, Y.; Rechtsman, M. C.; Chong, Y. D.; Khajavikhan, M.; Christodoulides, D. N.; Segev, M. Topological Insulator Laser: Theory. *Science*. **2018**, *359* (6381).
- (5) Sun, X. C.; Hu, X. Topological Ring-Cavity Laser Formed by Honeycomb Photonic Crystals. *Phys. Rev. B* **2021**, *103* (24).
- (6) He, X. T.; Liang, E. T.; Yuan, J. J.; Qiu, H. Y.; Chen, X. D.; Zhao, F. L.; Dong, J. W. A Silicon-on-Insulator Slab for Topological Valley Transport. *Nat. Commun.* **2019**, *10*, 872.
- (7) Li, R.; Bourgeois, M. R.; Cherqui, C.; Guan, J.; Wang, D.; Hu, J.; Schaller, R. D.; Schatz, G. C.; Odom, T. W. Hierarchical Hybridization in Plasmonic Honeycomb Lattices. *Nano Lett.* **2019**, *19*, 6435–6441.
- (8) Parappurath, N.; Alpegiani, F.; Kuipers, L.; Verhagen, E. Direct Observation of Topological Edge States in Silicon Photonic Crystals: Spin, Dispersion, and Chiral Routing. *Sci. Adv.* **2020**, *6* (10).

- (9) Gorlach, M. A.; Ni, X.; Smirnova, D. A.; Korobkin, D.; Zhirihin, D.; Slobozhanyuk, A. P.; Belov, P. A.; Alù, A.; Khanikaev, A. B. Far-Field Probing of Leaky Topological States in All-Dielectric Metasurfaces. *Nat. Commun.* **2018**, *9*, 909.
- (10) Hyun, W. J.; Lee, H. K.; Oh, S. S.; Hess, O.; Choi, C. G.; Im, S. H.; Park, O. O. Two-Dimensional TiO<sub>2</sub> Inverse Opal with a Closed Top Surface Structure for Enhanced Light Extraction from Polymer Light-Emitting Diodes. *Adv. Mater.* **2011**, *23* (16), 1846–1850.
- (11) Lan, N. X. V.; Moon, J.; Kang, T. H.; Wang, K.; Park, H. G.; Yi, G. R. Index-Matched Composite Colloidal Crystals of Core-Shell Particles for Strong Structural Colors and Optical Transparency. *Chem. Mater.* **2021**, *33* (5), 1714–1722.
- (12) Yeo, S. J.; Tu, F.; Kim, S. H.; Yi, G. R.; Yoo, P. J.; Lee, D. Angle- and Strain-Independent Coloured Free-Standing Films Incorporating Non-Spherical Colloidal Photonic Crystals. *Soft Matter* **2015**, *11* (8), 1582–1588.
- (13) Chen, Q.; Bae, S. C.; Granick, S. Directed Self-Assembly of a Colloidal Kagome Lattice. *Nature* **2011**, *469*, 381–384.
- (14) Gong, Z.; Hueckel, T.; Yi, G. R.; Sacanna, S. Patchy Particles Made by Colloidal Fusion. *Nature* **2017**, *550*, 234–238.
- (15) Diaz, J. A. A.; Oh, J. S.; Yi, G. R.; Pine, D. J. Photo-Printing of Faceted DNA Patchy Particles. *Proc. Natl. Acad. Sci. U. S. A.* **2020**, *117* (20), 10645–10653.
- (16) Choi, H. K.; Im, S. H.; Park, O. O. Fabrication of Unconventional Colloidal Self-Assembled Structures. *Langmuir* **2010**, *26* (15), 12500–12504.
- (17) Mukhopadhyay, R.; Al-Hanbali, O.; Pillai, S.; Hemmersam, A. G.; Meyer, R. L.; Hunter, A. C.; Rutt, K. J.; Besenbacher, F.; Moghimi, S. M.; Kingshott, P. Ordering

of Binary Polymeric Nanoparticles on Hydrophobic Surfaces Assembled from Low Volume Fraction Dispersions. *J. Am. Chem. Soc.* **2007**, *129*, 13390–13391.

(18) Khalil, K. S.; Sagastegui, A.; Li, Y.; Tahir, M. A.; Socolar, J. E. S.; Wiley, B. J.; Yellen, B. B. Binary Colloidal Structures Assembled through Ising Interactions. *Nat. Commun.* **2012**, *3*, 794.

(19) Galisteo-López, F.; Palacios-Lidón, E.; Castillo-Martínez, E.; López, C. Optical Study of the Pseudogap in Thickness and Orientation Controlled Artificial Opals. *Phys. Rev. B - Condens. Matter Mater. Phys.* **2003**, *68*, 115109.

(20) Baryshev, A. V.; Khanikaev, A. B.; Fujikawa, R.; Uchida, H.; Inoue, M. Polarized Light Coupling to Thin Silica-Air Opal Films Grown by Vertical Deposition. *Phys. Rev. B.* **2007**, *76*, 014305.

(21) Guo, R.; Hakala, T. K.; Törmä, P. Geometry Dependence of Surface Lattice Resonances in Plasmonic Nanoparticle Arrays. *Phys. Rev. B.* **2017**, *95*, 155423.

(22) Seo, I. C.; Kim, S.; Woo, B. H.; Chung, I. S.; Jun, Y. C. Fourier-Plane Investigation of Plasmonic Bound States in the Continuum and Molecular Emission Coupling. *Nanophotonics* **2020**, *9* (15), 4565–4577.

(23) Nozawa, K.; Gailhanou, H.; Raison, L.; Panizza, P.; Ushiki, H.; Sellier, E.; Delville, J. P.; Delville, M. H. Smart Control of Monodisperse Stöber Silica Particles: Effect of Reactant Addition Rate on Growth Process. *Langmuir* **2005**, *21* (4), 1516–1523.

(24) Todeschini, M.; Bastos Da Silva Fanta, A.; Jensen, F.; Wagner, J. B.; Han, A. Influence of Ti and Cr Adhesion Layers on Ultrathin Au Films. *ACS Appl. Mater. Interfaces* **2017**, *9* (42), 37374–37385.

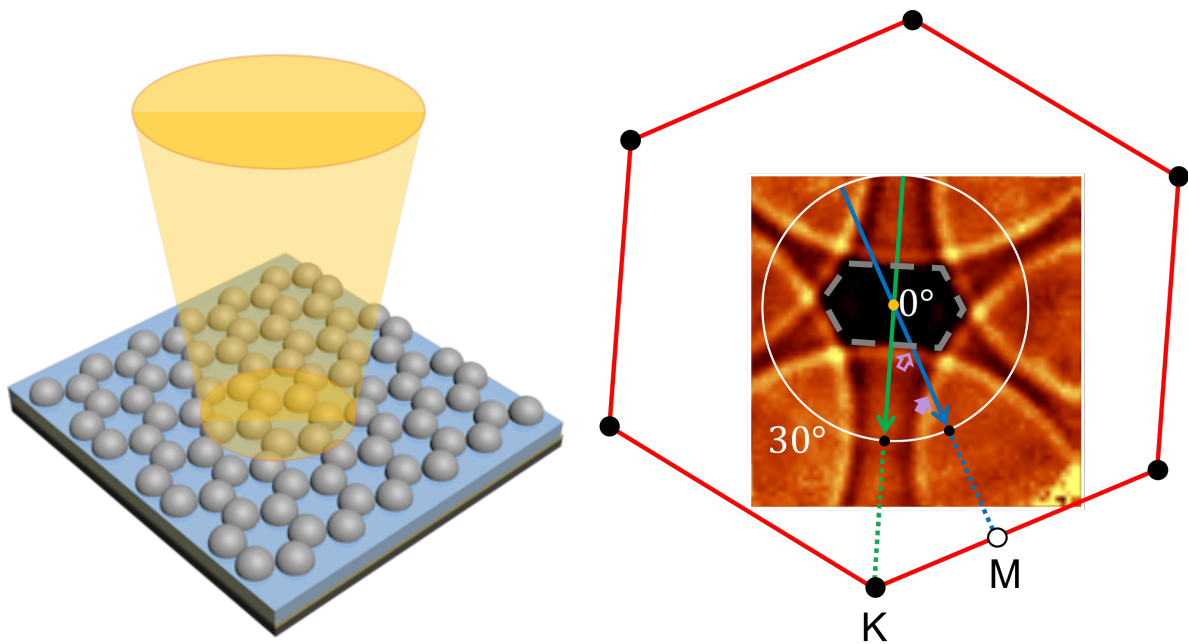
- (25) Suh, D.; Tak, H.; Choi, S. J.; Kim, T. II. Permeability- and Surface-Energy-Tunable Polyurethane Acrylate Molds for Capillary Force Lithography. *ACS Appl. Mater. Interfaces* **2015**, *7* (43), 23824–23830.
- (26) Fleck, N. A.; McMeeking, R. M.; Kraus, T. Convective Assembly of a Particle Monolayer. *Langmuir* **2015**, *31* (51), 13655–13663.
- (27) Kim, B. Q.; Qiang, Y.; Turner, K. T.; Choi, S. Q.; Lee, D. Heterostructured Polymer-Infiltrated Nanoparticle Films with Cavities via Capillary Rise Infiltration. *Adv. Mater. Interfaces* **2021**, *8* (3), 2001421.
- (28) Johnson, S.; Joannopoulos, J. Block-Iterative Frequency-Domain Methods for Maxwell's Equations in a Planewave Basis. *Opt. Express* **2001**, *8* (3), 173–190.
- (29) Nanophotonic FDTD Simulation Software-Lumerical <https://www.lumerical.com/products/fdtd/>. (accessed 2022-01-06).
- (30) Palik, E. D. *Handbook of Optical Constants of Solids*, Volume 1.; PALIK, E. D., Naval Research Laboratory, Washington, D. C., Eds.; Orlando : Academic Press, 1985. pp 57-73
- (31) P. B. Johnson and R. W. Christy. Optical Constant of the Nobel Metals. *Phys. Rev. B* **1972**, *6*, 4370.
- (32) Gierlinger, N.; Keplinger, T.; Harrington, M. Imaging of Plant Cell Walls by Confocal Raman Microscopy. *Nat. Protoc.* **2012**, *7*, 1694–1708.
- (33) Liz-marza, L. M.; Giersig, M.; Mulvaney, P. Synthesis of Nanosized Gold - Silica Core - Shell Particles. *Langmuir* **1996**, *12* (18), 4329–4335.
- (34) Suh, K. Y.; Choi, S. J.; Baek, S. J.; Kim, T. W.; Langer, R. Observation of High-Aspect-Ratio Nanostructures Using Capillary Lithography. *Adv. Mater.* **2005**, *17* (5), 560–564.

- (35) Flauraud, V.; Mastrangeli, M.; Bernasconi, G. D.; Butet, J.; Alexander, D. T. L.; Shahrabi, E.; Martin, O. J. F.; Brugger, J. Nanoscale Topographical Control of Capillary Assembly of Nanoparticles. *Nat. Nanotechnol.* **2017**, *12*, 73–80.
- (36) Dyogtyev, A. V.; Sukhoivanov, I. A.; De La Rue, R. M. Photonic Band-Gap Maps for Different Two Dimensionally Periodic Photonic Crystal Structures. *J. Appl. Phys.* **2010**, *107*, 013108.
- (37) Tan, B. J. Y.; Sow, C. H.; Koh, T. S.; Chin, K. C.; Wee, A. T. S.; Ong, C. K. Fabrication of Size-Tunable Gold Nanoparticles Array with Nanosphere Lithography, Reactive Ion Etching, and Thermal Annealing. *J. Phys. Chem. B* **2005**, *109* (22), 11100–11109.
- (38) Frisbie, S. P.; Chesnutt, C. F.; Holtz, M. E.; Krishnan, A.; De Peralta, L. G.; Bernussi, A. A. Image Formation in Wide-Field Microscopes Based on Leakage of Surface Plasmon-Coupled Fluorescence. *IEEE Photonics J.* **2009**, *1* (2), 153–162.
- (39) Vaskin, A.; Kolkowski, R.; Koenderink, A. F.; Staude, I. Light-Emitting Metasurfaces. *Nanophotonics* **2019**, *8* (7), 1151–1198.
- (40) Lozano, G.; Grzela, G.; Verschuuren, M. A.; Ramezani, M.; Rivas, J. G. Tailor-Made Directional Emission in Nanoimprinted Plasmonic-Based Light-Emitting Devices. *Nanoscale* **2014**, *6* (15), 9223–9229.

For Table of Contents Use Only

# Self-assembled Honeycomb Lattices of Dielectric Colloidal Nanospheres Featuring Photonic Dirac Cones

Yeongha Kim, Stephan Wong, Changwon Seo, Jeong Hoon Yoon, Gwan Hyun Choi, Jan  
Olthaus, Doris E. Reiter, Jeongyong Kim, Pil J. Yoo, Teun-Teun Kim, Sang Soon Oh, Gi-  
Ra Yi



## Supporting Information

# Self-assembled Honeycomb Lattices of Dielectric Colloidal Nanospheres Featuring Photonic Dirac Cones

Yeongha Kim<sup>a, ‡</sup>, Stephan Wong<sup>b, ‡</sup>, Changwon Seo<sup>c, ‡</sup>, Jeong Hoon Yoon<sup>a</sup>, Gwan Hyun Choi<sup>a</sup>,  
Jan Olthaus<sup>d</sup>, Doris E. Reiter<sup>d</sup>, Jeongyong Kim<sup>e</sup>, Pil J. Yoo<sup>a</sup>, Teun-Teun Kim<sup>c\*</sup>, Sang Soon  
Oh<sup>b\*</sup>, Gi-Ra Yi<sup>a,f\*</sup>

<sup>a</sup> School of Chemical Engineering, Sungkyunkwan University (SKKU), Suwon 16419, Republic of Korea.

<sup>b</sup> School of Physics and Astronomy, Cardiff University, Cardiff CF24 3AA, United Kingdom.

<sup>c</sup> Department of Physics and Energy Harvest-Storage Research Center (EHSRC), University of Ulsan, Ulsan 44610, Republic of Korea.

<sup>d</sup> Institute of Solid State Theory, University of Münster, 48149 Münster, Germany

<sup>e</sup> Department of Energy Science, Sungkyunkwan University, Suwon 16419, Republic of Korea

<sup>f</sup> Department of Chemical Engineering, Pohang University of Science and Technology (POSTECH), Pohang, Gyeongbuk 37673, Republic of Korea

\*Corresponding authors

E-mail: [yigira@postech.ac.kr](mailto:yigira@postech.ac.kr) (G.-R.Y.), [ohs2@cardiff.ac.uk](mailto:ohs2@cardiff.ac.uk) (S.S.O.), [tkim@ulsan.ac.kr](mailto:tkim@ulsan.ac.kr) (T.-T.K.)

‡ Y.K, S.W, and C.S contributed equally to this paper

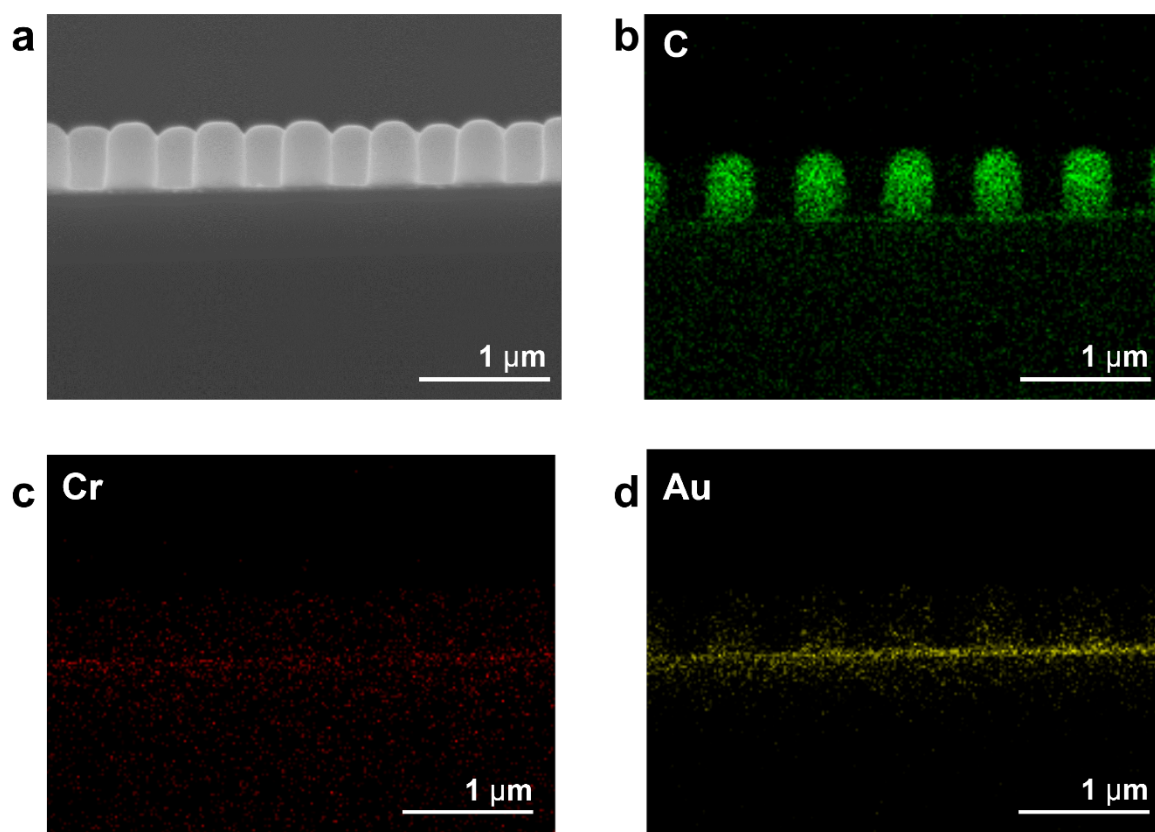


**Figure S1.** SEM cross-section image of hexagonal polystyrene pattern. We can see that all layers of (c) chromium, (d) gold, and (b) polystyrene are uniformly and well deposited. Silica nanoparticles will be assembled on this patterned substrate.

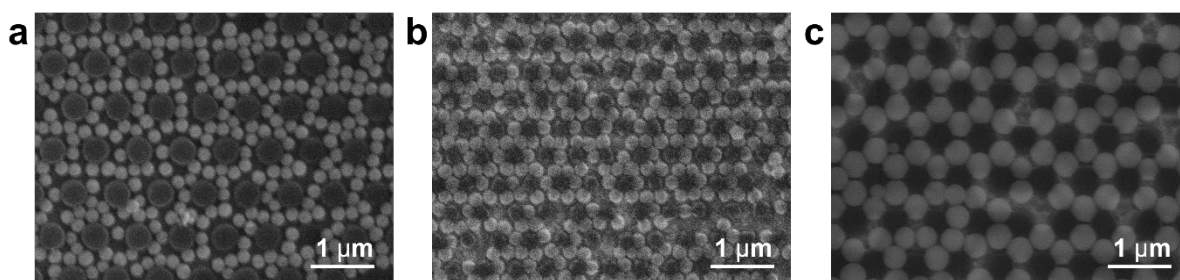


**Figure S2.** Various two-dimensional structures can be fabricated by changing only the particle size of Silica on the same pattern. We used (a) 160 nm, (b) 250 nm, (c) 400 nm sizes of Silica nanoparticles.

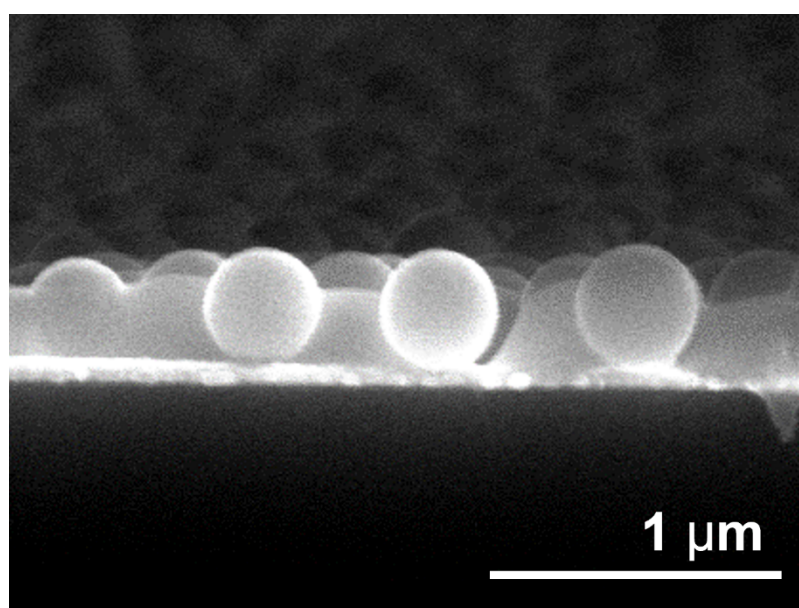


**Figure S3.** SEM cross-section image of silica honeycomb lattice. Hexagonal arrayed polystyrene patterns are slightly melted and hold the Silica nanoparticles.

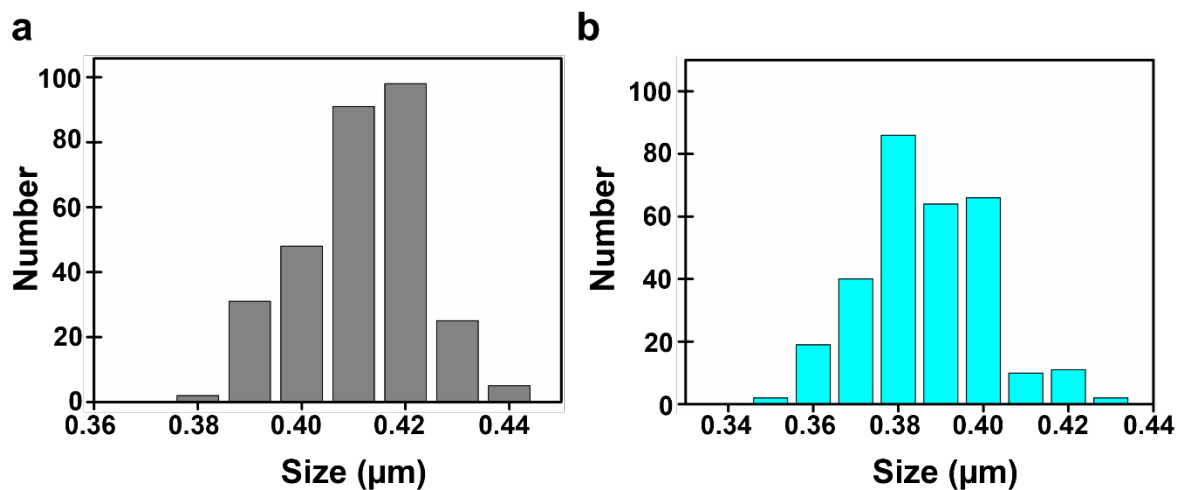


**Figure S4.** Histogram to prove uniformity of (a) silica nanoparticle size ( $400 \text{ nm} \pm 11 \text{ nm}$ ), and (b) diameter of polystyrene pattern ( $390 \text{ nm} \pm 14 \text{ nm}$ ).

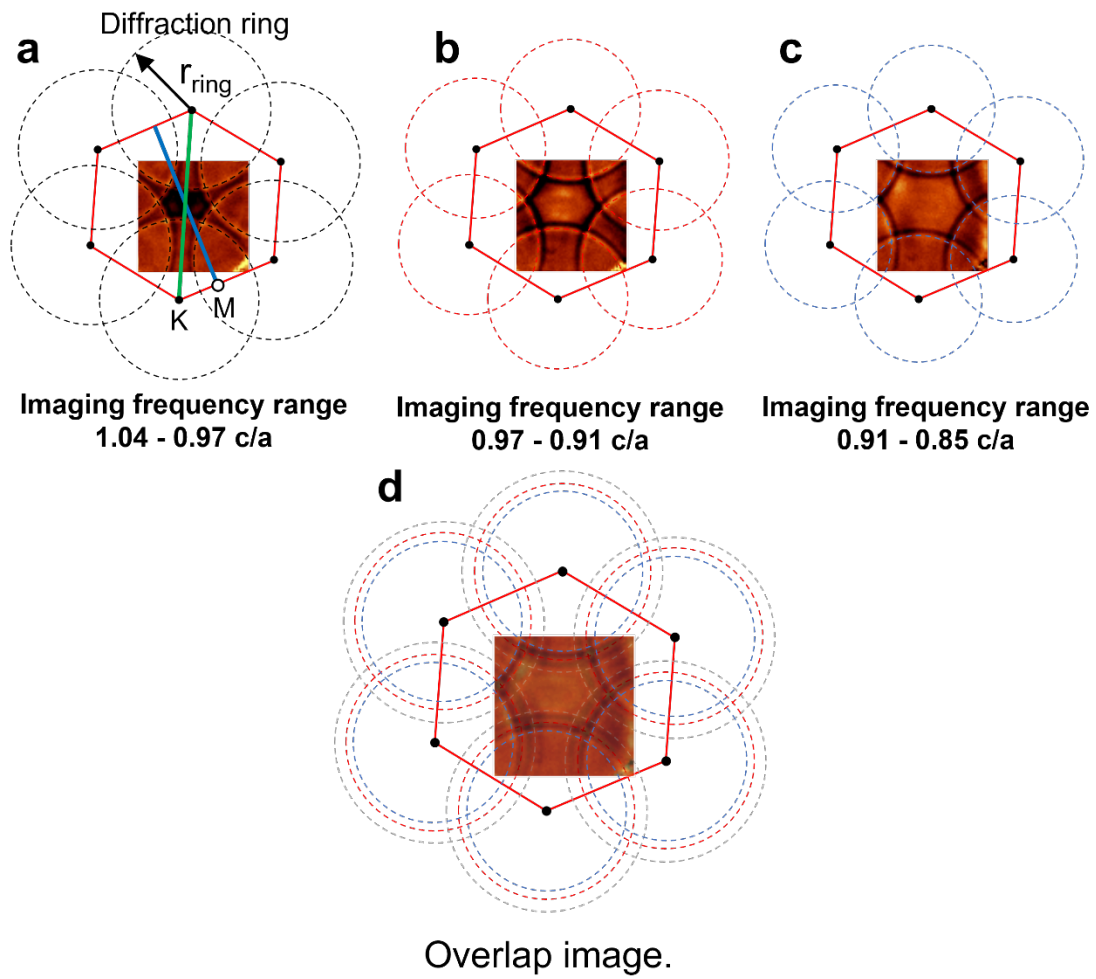


**Figure S5.** Diffraction rings and 1<sup>st</sup> Brillouin zone of honeycomb structure. (a), (b), and (c) show many diffraction rings with different radius ( $r_{\text{ring}}$ ) depending on the dip frequency. The inset maps are imaged by different frequency ranges with  $0.97 - 1.04 c/a$  (left),  $0.91 - 0.97 c/a$  (middle), and  $0.91 - 0.85 c/a$  (right), respectively. The black dots and red hexagon represent the K points and the 1<sup>st</sup> Brillouin zone of honeycomb structure. green and blue line show the K and M direction respectively. (d) Overlap image of (a), (b), and (c) with the diffraction rings. The concentric rings at K point and different radius depending on the dip frequencies are observed.